Studies of cross sections for collisions of electrons from hydride molecules: NH_3 and PH_3

Gurpreet Kaur,[1,2] Arvind Kumar Jain,[1] Harsh Mohan,[1] Parjit S. Singh,[2] Sunita Sharma,[3] and A. N. Tripathi[4]
[1]*Department of Physics, M. L. N. College, Yamuna Nagar, 135 001, Haryana, India*
[2]*Department of Physics, Punjabi University, Patiala, 147 002, Punjab, India*
[3]*Department of Chemistry, M. L. N. College, Yamuna Nagar, 135 001, Haryana, India*
[4]*Department of Physics, Indian Institute of Technology, Roorkee, 247 667, Uttarakhand, India*
(Received 12 September 2014; published 2 February 2015)

A parameter-free spherical complex optical potential approach in the fixed-nuclei approximation is applied here to calculate elastic differential, integral, and momentum-transfer cross sections as well as total (elastic plus inelastic) cross sections for the scattering of electrons from NH_3 and PH_3 molecules (i.e., nonmetallic hydrides) in the electron energy range of 0.1–100 eV. The projectile-target interaction is represented by a sum of a real and an imaginary potential. Present calculated results are compared with the available calculations and the experimental measurements. The quantitative features of the scattering parameters (such as Ramsauer-Townsend minimum and shape resonance structure), as observed in experiments, are well reproduced in the present study.

DOI: 10.1103/PhysRevA.91.022702 PACS number(s): 34.80.Bm, 34.90.+q

I. INTRODUCTION

The study of low-energy electrons with molecules like ammonia (NH_3) and phosphine (PH_3) is of interest in various physical processes occurring in the plasma physics, switching devices, interstellar space, atmospheric and radiation physics, etc. [1,2]. For example, it is well established that NH_3 has become a very important source of nitrogen atoms in the fabrication industries [3]. Similarly the PH_3 molecule also forms a major component in the fabrication of materials for nano- and optoelectronics [4]. Molecules of PH_3 are being used as a suitable source of phosphorus dopants in the realization of nano- and atomic-scale devices for quantum computing [5]. Apart from its use in semiconductor industries, recently PH_3 gas has been found in Saturn's troposphere [6] and its traces have been found in the lower and upper terrestrial troposphere of the earth [7,8]. Further, paddy fields throughout the rice growing stages were discovered as one of the main sources responsible for the production and emission of PH_3 gas in the atmosphere [9].

In recent years, the total cross sections for electron or positron collision with a large number of atoms and polyatomic molecules have been measured for the low ($\sim$1 eV) to keV energy range [10–12]. There exist some measurements for the elastic scattering of electrons by NH_3 and PH_3 molecules. The total cross sections for positron and electron collisions with NH_3 and H_2O were measured by Sueoka *et al.* [13] in the energy range 1$-$400 eV. Alle *et al.* [14] reported absolute differential cross section measurements for vibrationally elastic $e-NH_3$ scattering at incident energies from 2 to 30 eV. Szmytkowski *et al.* [15] measured total absolute cross sections for electron scattering on NH_3, OCS, and N_2O by using a linear transmission technique in the energy range 1–100 eV. Scattering of cold electrons by ammonia, hydrogen sulfide, and carbonyl sulfide was reported by Jones *et al.* [16]. They reported the experimental measurements for the total elastic and inelastic cross sections in different regions as 20 meV$-$10 eV for NH_3; 25 meV$-$10 eV for H_2S, and 15 meV$-$2.5 eV for OCS. Itikawa [17] presented a set of "recommended" values for the momentum-transfer cross sections for electron collisions with NH_3 molecules over the range 0.01$-$10 eV. In the case of the PH_3 molecule, Otvos and Stevenson [18] have measured electron-impact total ionization cross sections at 75 eV. Electron-impact ionization has been studied in PH_3 as a function of electron energy up to 180 eV by Mark and Egger [19]. Ariyasinghe *et al.* [20] have reported the total electron scattering cross sections of PH_3 and SiH_4 molecules for 90–3500 eV electrons by measuring the attenuation of the electron beam through a gas cell. In swarm experiments, Millican and Walker [21] have measured electron transport coefficients in phosphine. The absolute total scattering cross sections for electron collision have been measured by Szmytkowski *et al.* [22] in the incident electron energy range 0.5$-$370 eV by using a linear transmission experiment.

From a theoretical prespective, there exist several calculations for the elastic scattering of electrons by NH_3 and PH_3 molecules. Munjal and Baluja [23] calculated elastic differential, total, momentum-transfer, and excitation cross sections for electron impact on the NH_3 molecule using the $R-$matrix method in the energy range 0.025–20 eV. Jain [24] reported theoretical results on the total (elastic + inelastic) cross sections over the wide energy range 10–3000 eV by employing semiempirical spherical complex optical potentials for the electron-H_2O and -NH_3 systems. The elastic differential cross sections for $e-NH_3$ collisions were reported by Lino [25] using Schwinger variational principle at energies from 8.5 to 30 eV. Similar method at static-exchange level was used by Pritchard *et al.* [26] to calculate differential and momentum-transfer cross sections for elastic scattering of electrons by NH_3 for collision energies from 2.5 to 20 eV. A parameter-free model was used by Gianturco [27] for calculations of scattering cross sections for H_2S and NH_3 molecules in the energy region 0.1–20 eV. Rescigno *et al.* [28] performed a theoretical calculation of low-energy $e-NH_3$ scattering in which exchange and polarization effects have also been included in the complex Kohn (CK) variational technique at energies between 1 and 20 eV. Yuan and Zhang [29] reported total, differential, and momentum-transfer cross sections for the vibrationally elastic scattering of electrons from H_2O and NH_3 molecules in the energy range 0.5–20 eV. The fixed-nuclei and the adiabatic-rotation approximations were used

by Jain and Thompson [30] to calculate rotationally elastic, inelastic, and summed momentum-transfer cross sections for the electron-NH_3 scattering in the range 0.01–10 eV. In addition, we also have calculated elastic differential, total, and momentum-transfer cross sections in the energy range 100–1000 eV [31].

In the case of the PH_3 molecule, there are a few theoretical calculations, which have been performed using the Schwinger multichannel (SMC) method at various levels of approximation. The SMC is an *ab initio* variational method and is based on a stationary functional for the scattering amplitude. The scattering wave functions are calculated using quadratically integrable L^2 functions, and therefore, bound-state methodology is employed. Winstead *et al.* [32] calculated differential, total, and momentum-transfer cross sections for elastic scattering of $1-40$ eV electrons by PH_3 and AsH_3 using the SMC method. They found a low-energy shape resonance in the E symmetry of the C_{3v} point group. They used the static-exchange (SE) approximation and observed a shape resonance for PH_3 at 4 eV above the experimental value. The total cross sections for elastic scattering of low-energy electrons, i.e., $0.5-8$ eV by the hydrides PH_3, AsH_3, and SbH_3 molecules have been reported by Bettega and Lima [33]. They used the application of the SMC method with pseudopotentials at the static-exchange plus polarization level. Further, Bettega *et al.* [34] have also calculated total and differential cross sections for scattering of low-energy electrons from hydrides like PH_3, AsH_3, SbH_3, SnH_4, TeH_2, and HI from 10 to 30 eV by employing the SMC method with norm-conserving pseudopotentials. Elastic and rotational excitation cross sections were computed by Varella *et al.* [35] at the static-exchange approximation for the electron collision with NH_3, PH_3, AsH_3, and SbH_3 in the energy range 7.5–30 eV. Limbachiya *et al.* [36] reported total (elastic plus electronic excitation) cross sections for electron impact on NH_3, H_2S, and PH_3 over the energy range from 0.01 eV to 2 keV. There also exist calculations of total, differential, and momentum-transfer cross sections by Yuan and Zhang [37] for the vibrationally elastic scattering of electron impact from H_2S and PH_3 molecules in the energy range 0.1–50 eV. They used the spherical approximations for molecular wave functions. Jain and Baluja [38] employed an optical model potential to estimate the total (elastic + inelastic) electron scattering cross sections in a wide energy range (10–5000 eV) from several diatomic and polyatomic molecular targets. The total elastic cross section for scattering of electrons by phosphine molecules has been calculated by Munjal and Baluja [39] using the $R-$matrix method for incident electron energies in the range 0.025–15 eV.

In the present work, the spherical complex optical potential (SCOP) approach has been used to compute the differential, elastic, total (elastic plus inelastic), and momentum-transfer cross sections for electrons scattering from NH_3 and PH_3 molecules in the energy range 0.1–100 eV. To our knowledge, there is a paucity of results for NH_3 and PH_3 using modified semiclassical exchange potential in the energy range considered here. The aim of this paper is to study the role of modified semiclassical exchange potential and absorption potential in this energy region using the optical model potential approach.

II. THEORETICAL METHODOLOGY

Both ammonia and phosphine molecules belong to the C_{3v} symmetry point group (electronic $^1A_1$ ground state) with the electronic configuration $1a_1^2 2a_1^2 1e^4 3a_1^2$ and $1a_1^2 1e^4 2a_1^2 3a_1^2 4a_1^2 2e^4 5a_1^2$, respectively. A single-center expansion technique (see Thompson and Gianturco [40]) with nitrogen or phosphorous atom at the center is employed for all orbitals in the near–Hartree-Fock limit using experimental values for nuclear geometry (bond length = 1.012 Å and bond angle = 106.7° for NH_3; bond length = 1.421 Å and bond angle = 93.3° for PH_3). The pivotal quantity in the calculations of the optical potential is the charge density $\rho(\vec{r})$ which is calculated from the single-center wave function with a large number of terms in the expansion of each bound orbital (for details, see Ref. [41]). The $\rho(\vec{r})$ is then expanded in terms of the symmetric A_1 irreducible representation of the molecular C_{3v} point group; i.e.,

$$\rho(\vec{r}) = \sum \bar{\rho}_{LH}(\vec{r}) X_{LH}^{A_1}(\hat{r}). \tag{1}$$

In the spherical approximation [42,43], only the first term ($L = 0, H = 1$) of the expansion of Eq. (1) is needed in order to evaluate all of the three local potentials, namely, the static (V_{st}), the exchange (V_{ex}), and the polarization (V_{pol}). An explicit expression for $V_{st}(\vec{r})$ is given in the literature (see, for example, Gianturco and Jain [44]).

The modified semiclassical exchange (MSCE) potential for $V_{ex}(\vec{r})$ is taken from Gianturco and Scialla [45]:

$$V_{ex}^{MSCE}(\vec{r}) = \frac{1}{2}\left\{E - V_{st}(\vec{r}) + \frac{3}{10}[3\pi^2\rho(\vec{r})]^{2/3}\right\} - \frac{1}{2}\left(\left\{E - V_{st}(\vec{r}) + \frac{3}{10}\left[3\pi^2\rho(\vec{r})\right]^{2/3}\right\}^2 + 4\pi^2\rho(\vec{r})\right)^{1/2}. \tag{2}$$

The calculation of an actual polarization potential which provides the second- and higher-order effects in the electron-molecule interaction is rather a challenging task. A common approach has been to derive it from its exact asymptotic form ($-\alpha_0/2r^4$, where α_0 is the dipole polarizability of the target in atomic units). However, such a scheme is not always satisfactory and demands a prior knowledge of the system under investigation. During the last few years, various authors have proposed an approximate parameter-free polarization potential which is based on the correlation energy of the target. The philosophy of the correlation polarization (CP) potential is quite simple. According to Connell and Lane [46], the correlation polarization potential is obtained in the whole radial region by smoothly joining the correlation energy function and the asymptotic form $-\alpha_0/2r^4$ (α_0, the dipole polarizability of NH_3 is 15.0 a.u. and PH_3 is 32.67 a.u.) where they cross each other for the first time (the crossing point occurs at 3.94 a.u. for NH_3 and 4.68 a.u. for PH_3). The functional form of the correlation polarization potential in the inner region of the interaction is derived from an approximate local correlation energy which is obtained in terms of charge density $\rho(\vec{r})$. Following Padial and Norcross [47] and Gianturco *et al.* [48], the correlation potential energy for various ranges of radial

distance (r) is as

$$V_{\rm cop}(\vec{r}) = \begin{cases} 0.0311\ln r_S + 0.006 r_S \ln r_S - 0.015 r_S - 0.0584, & r_S \leqslant 0.7 \\ 0.02224\ln r_S - 0.07356, & 0.7 \leqslant r_S \leqslant 10.0 \\ -0.584 r_S^{-1} + 1.988 r_S^{-3/2} - 2.45 r_S^{-2} - 0.733 r_S^{-5/2}, & 10.0 \leqslant r_S \end{cases}, \tag{3}$$

where $r_S(\vec{r}) = [\frac{3}{4\pi\rho(\vec{r})}]^{1/3}$.

The imaginary part of the optical potential is the absorption potential ($V_{\rm abs}$). It represents the combined effect of all the inelastic channels. Here, we employ the absorption potential as discussed by Blanco and Garcia [49]. It was observed that the use of this potential significantly improved the results [49,50]. Blanco and Garcia [49] reviewed the derivation of the original quasifree-scattering model given by Staszewska *et al.* [51] and found an error in it. The correct absorption potential is exactly one half that of the Staszewska *et al.* [51] potential. Furthermore, they [49] introduced an addition term (known as the corrective term) based on the Mott scattering formula in the absorption potential. Therefore, the final expression for the absorption potential is a sum of the two terms

$$V_{\rm abs}(\vec{r}) = V^R_{\rm abs}(\vec{r}) + V^C_{\rm abs}(\vec{r}), \tag{4}$$

where

$$V^R_{\rm abs}(\vec{r}) = -\frac{2V_{\rm loc}}{15\pi\, p^2} H\left(p^2 - k_f^2 - 2\Delta\right)(A_1 + A_2 + A_3), \tag{5}$$

with

$$\begin{aligned} V_{\rm loc} &= [2(E - V_{\rm st} - V_{\rm ex} - V_{\rm pol})]^{1/2}, \\ k_f &= [3\pi^2\rho(\vec{r})]^{1/3}, \\ A_1 &= 5k_f^3/2\Delta, \\ A_2 &= -k_f^3\left(5p^2 - 3k_f^2\right)/\left(p^2 - k_f^2\right)^2, \\ A_3 &= H(\delta)\,(2\delta^{5/2}p^5)/\left(p^2 - k_f^2\right)^2, \\ \delta &= 2\left(k_f^2 + \Delta\right)/p^2 - 1. \end{aligned}$$

Here $H(x)$ is a Heaviside function defined by

$$H(x) = \begin{cases} 1, & x \geqslant 0 \\ 0, & x < 0 \end{cases}. \tag{6}$$

By varying the value of Δ (free parameter) in $V_{\rm abs}$, one can improve the cross sections relative to experimental measurements. However, we have fixed Δ equal to the threshold energy for electronic excitation of the target molecule. For the present calculations, the value of Δ is taken [36] as 6.89 eV for NH_3 and 6.42 eV for PH_3.

The corrective term in the absorption potential ($V^C_{\rm abs}$) is given by

$$V^C_{\rm abs}(\vec{r}) = \frac{2V_{\rm loc}}{\pi\, p} H\left(p^2 - k_f^2 - 2\Delta\right) \times [f_\delta(k_f/p) - f_\delta(H(\delta)\delta^{1/2})], \tag{7}$$

where

$$f_\delta(x) \cong \frac{x(1-\delta)}{4(1-x)} + \frac{1}{16}[11 - x + (x-3)\delta]\log(1-x) + (a_1 - \delta b_1)x + (a_2 - \delta b_2)x^2, \tag{8}$$

with $a_1 = 0.4353$, $a_2 = 0.01233$, $b_1 = -0.1084$, and $b_2 = 0.05691$.

Finally, the total optical potential is

$$V_{\rm opt}(\vec{r}) = V_{\rm Re}(\vec{r}) + i\, V_{\rm Im}(\vec{r}), \tag{9}$$

where

$$V_{\rm Re}(\vec{r}) = V_{\rm st}(\vec{r}) + V_{\rm ex}(\vec{r}) + V_{\rm pol}(\vec{r})$$

and

$$V_{\rm Im}(\vec{r}) = V_{\rm abs}(\vec{r}).$$

It is now a standard procedure to compute the lth partial-wave phase shifts from the solution of the following second-order differential equation:

$$\left[\left(\frac{d^2}{dr^2}\right) + k^2 - \frac{l(l+1)}{r^2} - V_{\rm opt}(\vec{r})\right] f_l(k\vec{r}) = 0. \tag{10}$$

We employ the variable-phase approach (VPA) (Ref. [52]) to find the solution of the above equation. The corresponding quantities' elastic differential cross section (DCS), integral cross section ($\sigma_{\rm el}$), and momentum-transfer cross section (σ_m)

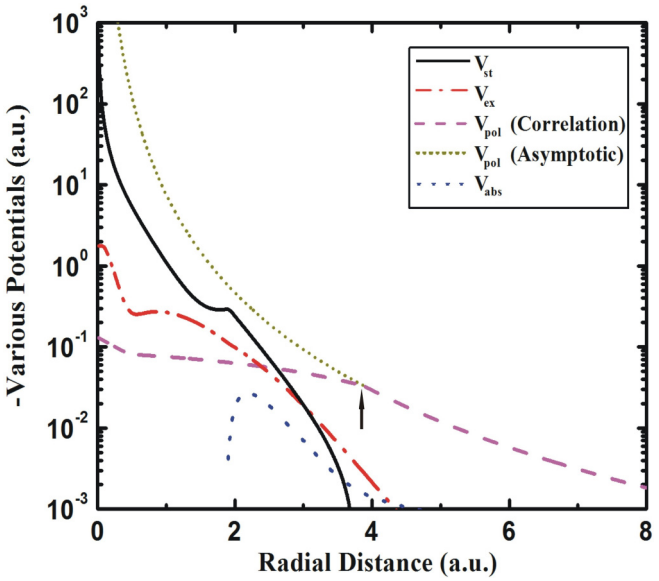

FIG. 1. (Color online) Various components of the interaction potentials for $e-NH_3$ scattering. Black solid line, static potential; red dashed-dot line, modified semiclassical exchange potential (at 30 eV); magenta dashed line, correlation polarization potential; dark yellow short dot line, asymptotic polarization potential; blue dot line, absorption potential (at 30 eV).

along with total (elastic plus inelastic) cross section (σ_t) are then easily obtained from the S matrix at each energy. All our cross sections have converged with respect to the number of partial waves.

III. RESULTS AND DISCUSSION

A. Electron scattering from ammonia, NH_3

Before we present our calculations on the cross sections of the $e-NH_3$ system, it is worthwhile to examine the behavior of the radial shapes of the potentials. They are displayed in Fig. 1. The static interaction dominates all the other interactions (exchange and polarization) up to $r = 2.62$ a.u. well outside the region of H nuclei. Beyond this distance, the correlation polarization dominates over both the static and exchange interactions. The exchange term remains weaker than the static potential up to $r \sim 3.05$ a.u. (see Fig. 1). We have also exhibited the absorption potential at 30 eV. We observed that the absorption effects exist only in the outer region of the target. However, the range of absorption potential is not as

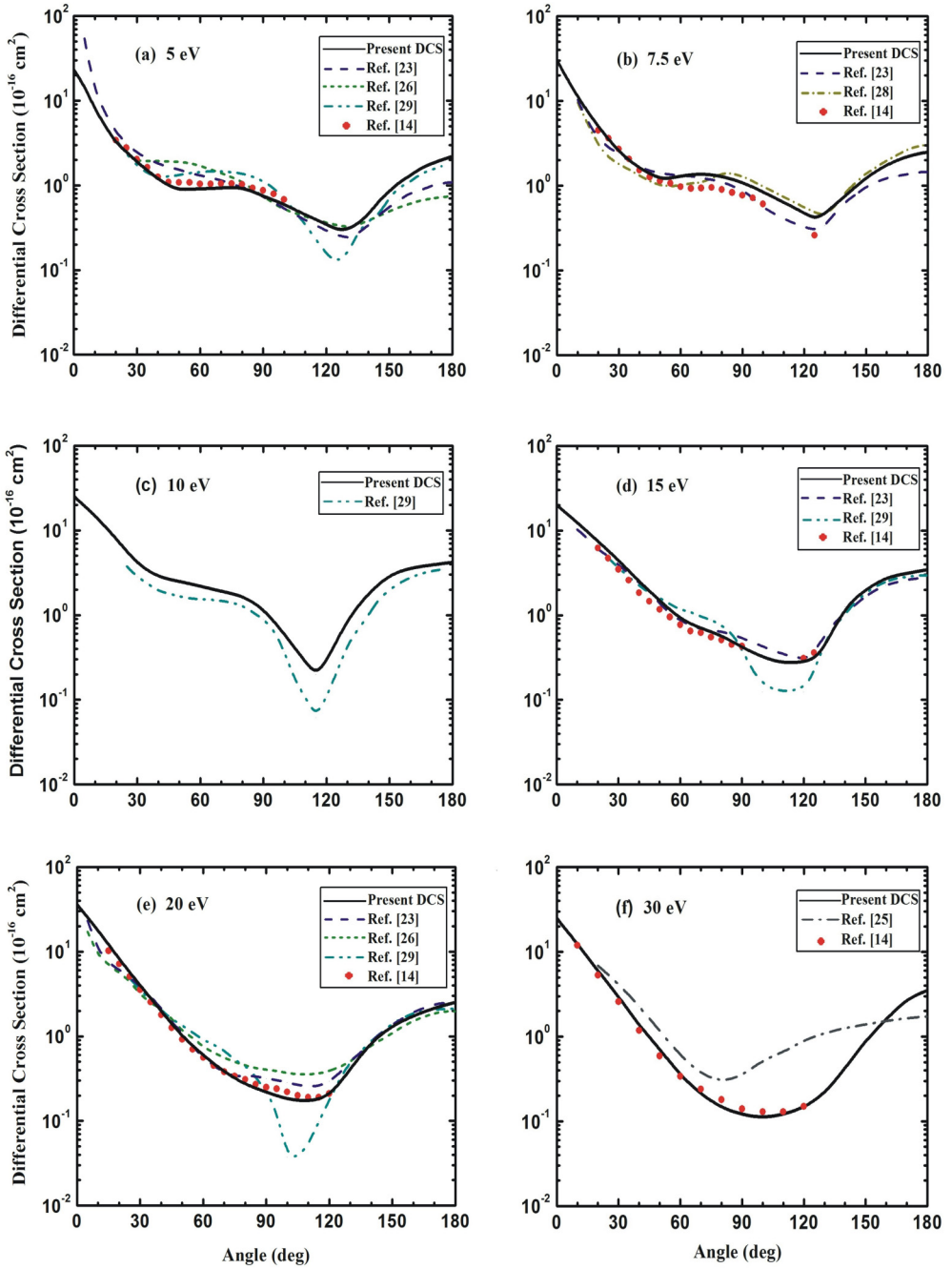

FIG. 2. (Color online) Differential cross sections for $e-NH_3$ scattering at energies (a) 5, (b) 7.5, (c) 10, (d) 15, (e) 20, and (f) 30 eV. Present calculations: Black solid line, elastic DCS. Other calculations: Navy blue dashed line, Munjal and Baluja [23]; dark gray dashed-dot line, Lino [25]; olive short dashed line, Pritchard *et al.* [26]; dark yellow short dashed-dot line, Rescigno *et al.* [28]; dark cyan dashed-dot-dot line, Yuan and Zhang [29]. Experimental data: Red filled circles, Alle *et al.* [14].

large as that of the polarization potential which asymptotically behaves like $1/r^4$.

In this paper, we present elastic differential cross sections (DCS) only at those energies where both experimental as well as other theoretical results were available. Therefore, in Figs. 2(a)–2(f) DCS are displayed at energies 5, 7.5, 10, 15, 20, and 30 eV respectively. Note that in the present fixed-nuclei approximation, the DCS are divergent in the forward scattering. The experimental DCSs of Alle *et al.* [14] are available at all of these energies except at an energy of 10 eV. We also compare our DCS with the theoretical calculations of Munjal and Baluja [23], Lino [25], Pritchard *et al.* [26], Rescigno *et al.* [28], and Yuan and Zhang [29].

At 5 eV [Fig. 2(a)], our results are in good agreement with the experimental measurements of Alle *et al.* [14] up to 40°; thereafter our results are lower by about 15%. However, the results of Yuan and Zhang [29] overestimate in the angular region up to 100°. We have also compared our results with the calculations of Munjal and Baluja [23], and Pritchard *et al.* [26], along with Rescigno *et al.* [28]. A broad minimum appears between 110° and 140° which is almost at a similar position, i.e., at a scattering angle around 125° as shown in the calculations of other workers.

In Fig. 2(b) DCS are shown at an energy of 7.5 eV. The present calculations reproduce the experimental measurements [14] very well up to $\theta \leqslant 50°$. Thereafter they overestimate the measurements by about 15%. We have displayed our DCS results at 10 eV in Fig. 2(c) along with calculations of Yuan and Zhang [29]. We notice a similarity between our results and the calculation of Yuan and Zhang [29]. The dip in the cross sections at 115° indicates the dominance of $p-$wave behavior of the scattered electron. Moving to the next higher energies, i.e., 15 and 20 eV [see Figs. 2(d) and 2(e)], our results are in good agreement with the experimental measurements in the entire angular region. Finally, in Fig. 2(f), DCS are illustrated at energy 30 eV. These are compared with the experimental measurement of Alle *et al.* [14] along with Schwinger variational principle plane wave (SVPPW) calculations of Lino [25]. At this energy, our DCS results agree well with the experimental measurements of Alle *et al.* [14] in shape and magnitude in the entire angular region.

We have also calculated elastic integral cross sections ($\sigma_{\rm el}$) as well as total (elastic plus inelastic) cross sections (σ_t) in the energy range 0.1–100 eV. A real comparison of our cross sections and experimental data of Szmytkowski *et al.* [15] along with the measurements of Sueoka *et al.* [13] and Alle *et al.* [14] is presented in Figs. 3(a) and 3(b). The theoretical calculations for the elastic cross sections performed by Munjal and Baluja [23] at $R-$matrix level and Yuan and Zhang [29] are also shown in this figure. Before we discuss our results, we would like to point out that only in the lower-energy region (i.e., <20 eV), the exchange and polarization interactions play an important role. Above 20 eV, the contribution of both the exchange and polarization terms seems to be constant which is due to the fact that the correlation polarization potential is energy independent. Further, below the electronic excitation threshold energy, the imaginary part [$V_{\rm abs}$] of the optical potential does not play any role. The absorption potential appears only at energies above the threshold energy. It is clear from Fig. 3(a) that at energies between 3 and 7 eV,

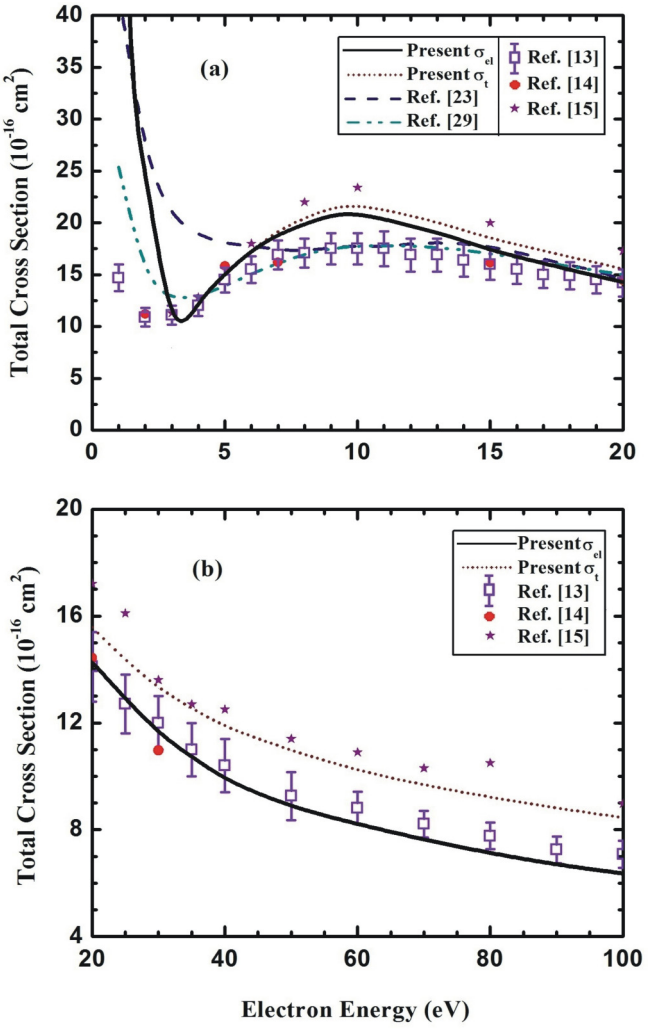

FIG. 3. (Color online) Total cross sections for $e-NH_3$ scattering in the energy range (a) 0.1–20 eV and (b) 20–100 eV. Present results: Black solid line, $\sigma_{\rm el}$ results; wine short dot line, σ_t results. Other calculations: Navy blue dashed line, Munjal and Baluja [23]; dark cyan dashed-dot-dot line, Yuan and Zhang [29]. Experimental data: Violet open squares with error bars, Sueoka *et al.* [13]; red filled circles, Alle *et al.* [14]; purple filled stars, Szmytkowski *et al.* [15].

our $\sigma_{\rm el}$ results are in agreement with the measurements of Szmytkowski *et al.* [15], Sueoka *et al.* [13], and Alle *et al.* [14]. The only difference between the present results and experimental data is observed below 3 eV. Since NH_3 has a permanent dipole moment (1.46 D), the cross sections at low energy are quite high. In view of this, the disagreement between theory and experiment for collision energies below 3 eV is not very surprising. All the theoretical calculations and experimental measurements exhibit a broad hump around 9 eV. Our σ_t cross sections are about 8% lower than the measurements of Szmytkowski *et al.* [15]. Figure 3(b) displays cross sections in the energy range between 20 and 100 eV. In this energy region, we present both our $\sigma_{\rm el}$ and σ_t cross sections along with experimental measurements of Sueoka *et al.* [13], Alle *et al.* [14], and Szmytkowski *et al.* [15]. Theoretical calculations of other researchers are not available for comparison in this energy region. It is clearly seen that

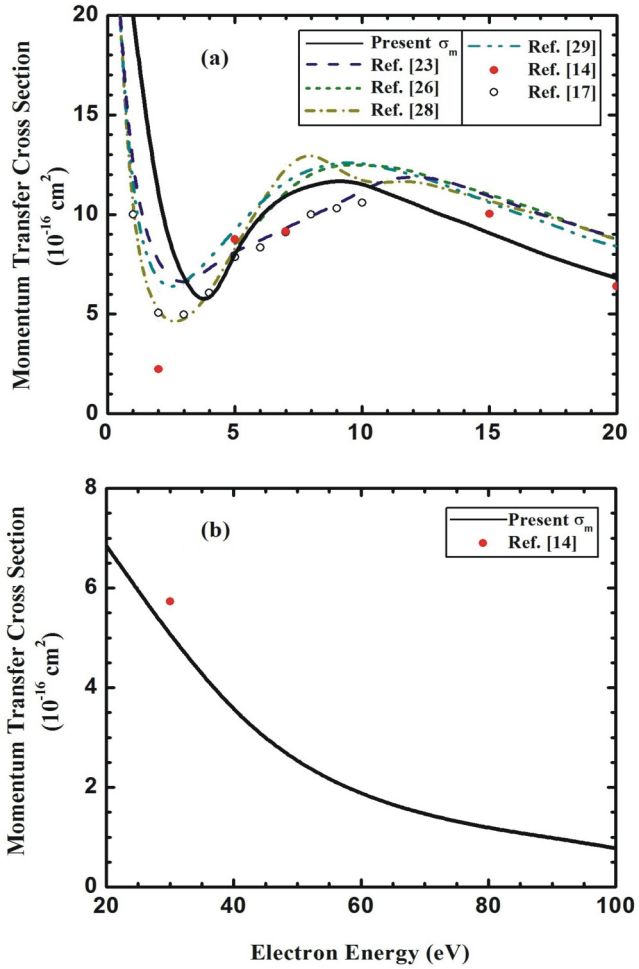

FIG. 4. (Color online) Momentum-transfer cross sections for $e-NH_3$ scattering in the energy range (a) 0.1–20 eV and (b) 20–100 eV. Present results: Black solid line, elastic σ_m results. Other calculations: Navy blue dashed line, Munjal and Baluja [23]; olive short dashed line, Pritchard *et al.* [26]; dark yellow short dashed-dot line, Rescigno *et al.* [28]; dark cyan dashed-dot-dot line, Yuan and Zhang [29]. Experimental data: Red filled circles, Alle *et al.* [14]; black open circles, recommended values of Itikawa [17].

the inclusion of the imaginary part significantly improves the results. Our calculated σ_t results are in very good agreement with the measurements of Szmytkowski *et al.* [15], whereas our σ_{el} results are in reasonable agreement with that of Sueoka *et al.* [13]. Further, it has been noticed that the contribution from the V_{abs}^{C} term decreases with the increase in energy above 50 eV. In Fig. 4(a), the present results of elastic momentum-transfer cross sections (σ_m) are compared with the experimental measurements of Alle *et al.* [14] and again with the theoretical calculations of Munjal and Baluja [23], Pritchard *et al.* [26], Rescigno *et al.* [28], Yuan and Zhang [29], and "recommended" values of Itikawa [17] in the energy region up to 20 eV. Momentum-transfer cross sections represent backward scattering contributions in collision dynamics. They play an important role in the study of a swarm of electrons drifting through a molecular charge cloud. There is a good scatter in the various calculations by other workers. However, our results are in qualitative agreement with the recommended

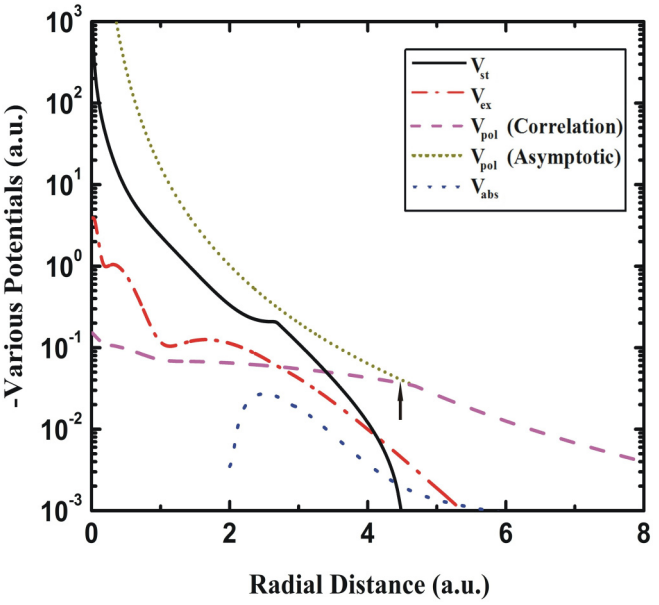

FIG. 5. (Color online) Same legend as in Fig. 1 except for $e-PH_3$ scattering.

values of Itikawa [17]. Figure 4(b) illustrates the σ_m cross sections in the energy region 20–100 eV. There is a paucity of experimental data as well as theoretical calculations of momentum-transfer cross sections in this energy region.

B. Electron scattering from phosphine, PH_3

The various components of the interaction terms for the $e-PH_3$ system are displayed in Fig. 5. These components show similar behavior as that of the NH_3 molecule. In the case of the PH_3 molecule, we have presented elastic DCS on the same energies as those for NH_3 molecules. Here DCS have been compared with the available calculations of Winstead *et al.* [32], Battega *et al.* [34], and Yuan and Zhang [37]. Perhaps there are no experimental data available for DCS of the PH_3 molecule at these energies to further assess the accuracy of any of these theoretical calculations. Our DCS for the $e-PH_3$ scattering system are shown in Figs. 6(a)–6(f). These show two minima and an intervening maximum. These arise due to the interference of various partial waves. At 5 eV [see Fig. 6(a)], a calculation of Yuan and Zhang [37] is available for the comparison of our DCS results. Our results show similarity with those of Yuan and Zhang [37] in shape and magnitude except for a minor difference at the middle angles. The difference in results may be due to the choice of exchange potential formalism. In Fig. 6(b), DCS are plotted at an energy 7.5 eV. In this figure, we also present the result of Winstead *et al.* [32] which is available at energy 8 eV. It is clear that the calculations of Winstead *et al.* [32] are quite similar to our DCS results. In this figure, it is observed that the resulting DCS are characterized by a dip in the angular distribution at the scattering angles around 75° and 130°. The dips arise due to the destructive interference of various partial waves at such low energy. This trend is continued for other higher energies, i.e., 10, 15, and 20 eV [see Figs. 6(c)–6(e), respectively] and is similar to the results of Yuan and Zhang [37]. As the

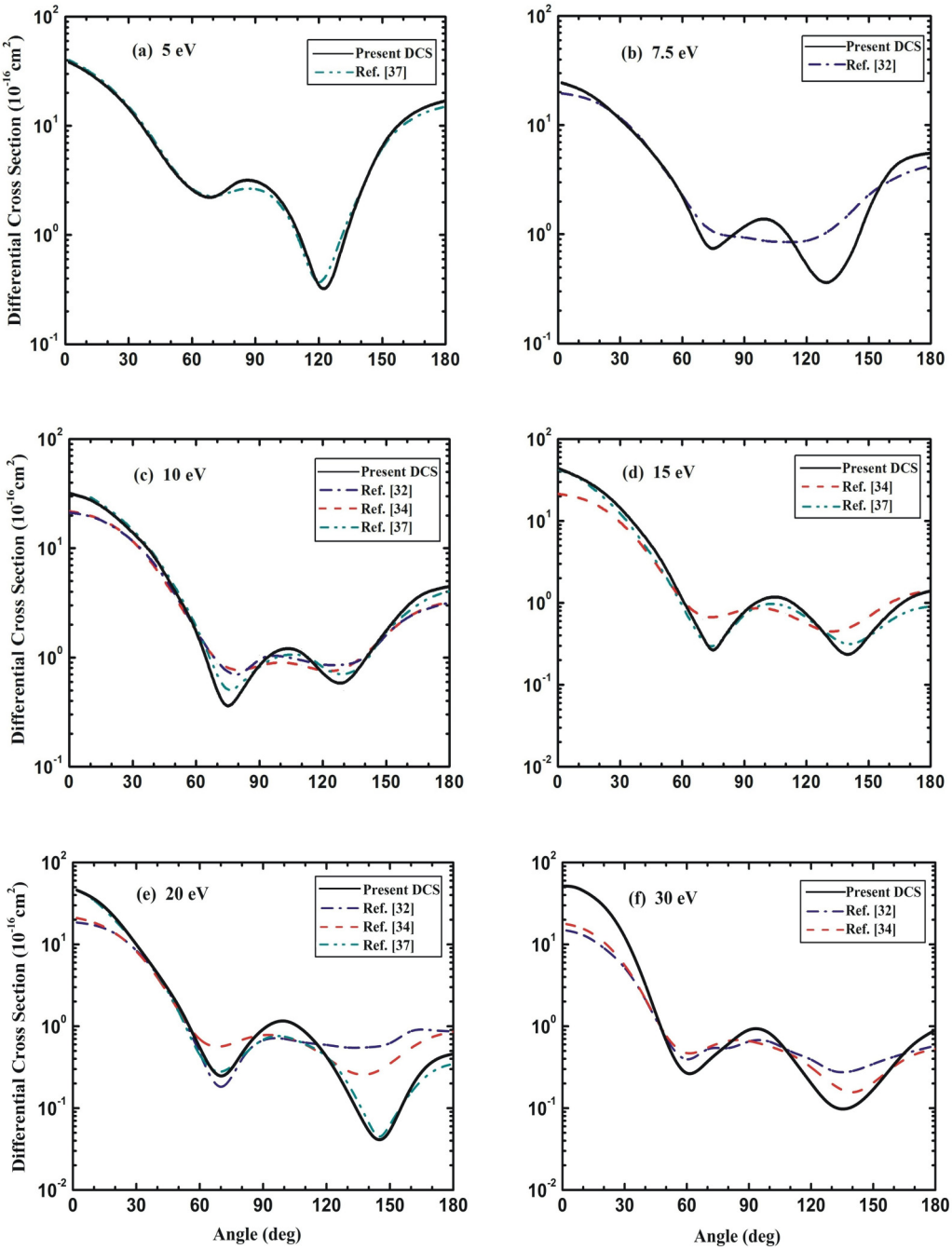

FIG. 6. (Color online) Differential cross sections for $e-PH_3$ scattering at energies (a) 5, (b) 7.5, (c) 10, (d) 15, (e) 20, and (f) 30 eV. Present results: Black solid line, elastic DCS. Other calculations: Royal blue dashed-dot line, Winstead *et al.* [32]; red dashed line, Battega *et al.* [34]; dark cyan dashed-dot-dot line, Yuan and Zhang [37].

energy increases, the dip positions are shifted towards higher scattering angles. The broad humps exhibited near the middle scattering angles clearly indicate the presence of hydrogen (hydrogen bonds). Further, it has been noticed that calculated DCS of Winstead *et al.* [32] and Battega *et al.* [34] also show similar behavior. The difference in forward direction is due to the dipole nature of the PH_3 molecule. Finally, in Fig. 6(f), DCS results are presented along with the calculations of Winstead *et al.* [32] and Battega *et al.* [34]. All the calculations produce dips around 60° and 135°. If the p wave is dominant then we expect a dip at 90°. Due to the presence of s and d waves which dominate at low energies, the dip due to the p wave is broken into two portions.

Figures 7(a) and 7(b) show both our σ_{el} and σ_t cross sections for the $e-PH_3$ system along with experimental measurements of Szmytkowski *et al.* [22] and theoretical calculations of Winstead *et al.* [32], Limbachiya *et al.* [36], Yuan and Zhang [37], Jain and Baluja [38], and Munjal and Baluja [39]. In Fig. 7(a), cross sections are presented up to 20 eV. Our σ_{el} results reproduce the Ramsauer-Townsend

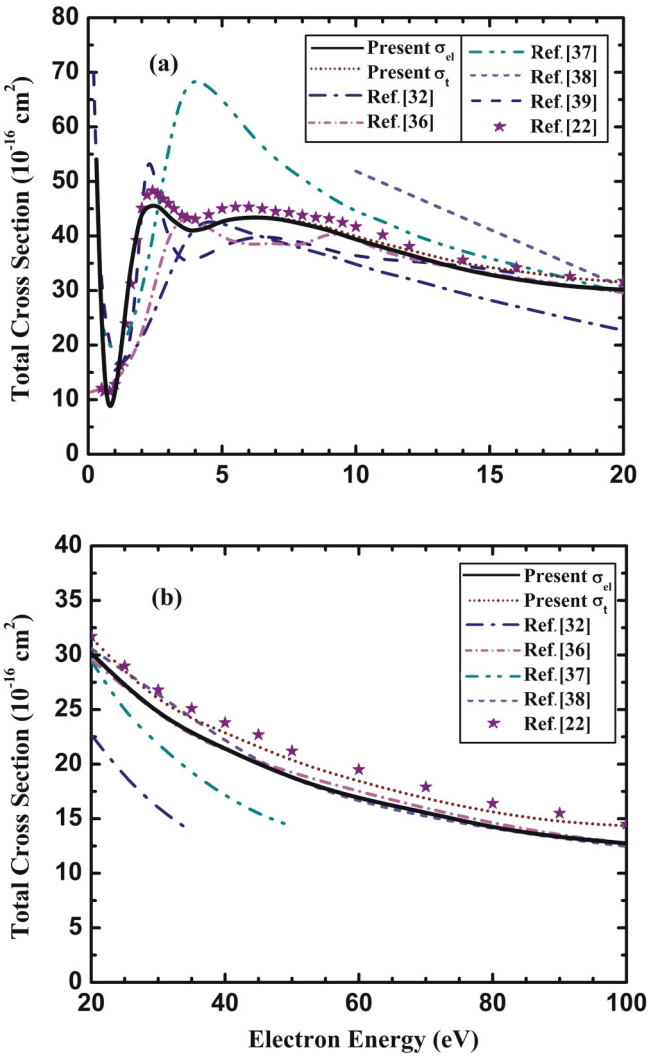

FIG. 7. (Color online) Total cross sections for $e-PH_3$ scattering in the energy range (a) 0.1–20 eV and (b) 20–100 eV. Present results: Black solid line, σ_{el} results; wine short dot line, σ_t results. Other calculations: Royal blue dashed-dot line, Winstead *et al.* [32]; magenta short dashed-dot line, Limbachiya *et al.* [36]; dark cyan dashed-dot-dot line, Yuan and Zhang [37]; violet short dashed line, Jain and Baluja [38]; navy blue dashed line, Munjal and Baluja [39]. Experimental data: Purple filled stars, Szmytkowski *et al.* [22].

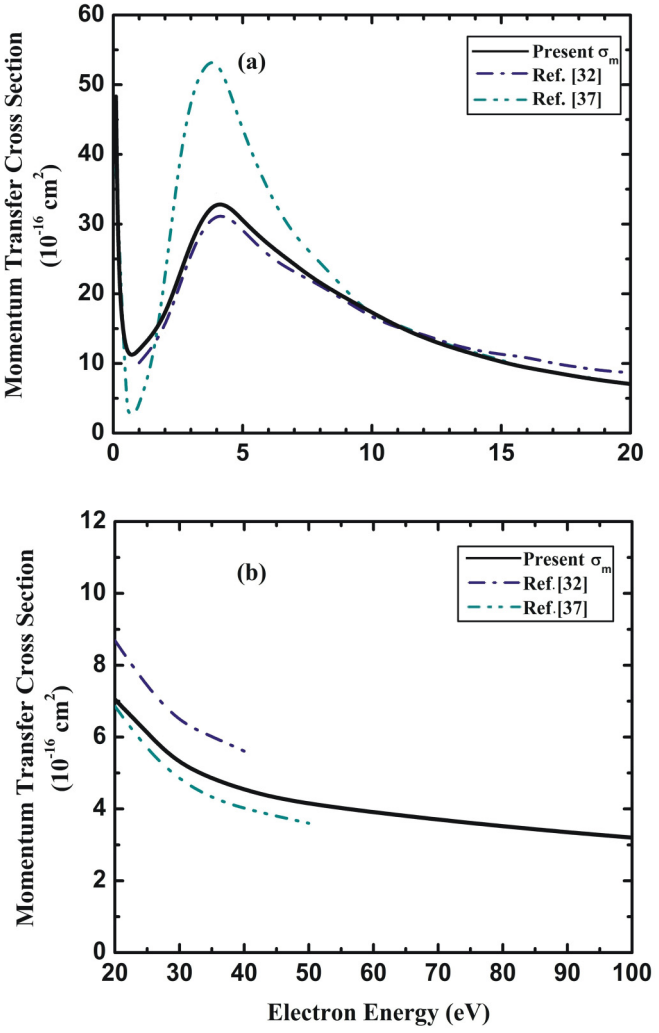

FIG. 8. (Color online) Momentum-transfer cross sections for $e-PH_3$ scattering in the energy range (a) 0.1–20 eV and (b) 20–100 eV. Present results: Black solid line, elastic σ_m results. Other calculations: Royal blue dashed-dot line, Winstead *et al.* [32]; dark cyan dashed-dot-dot line, Yuan and Zhang [37].

minima at 0.8 eV which is at a similar position as found in experimental measurements of Szmytkowski *et al.* [22]. We detect a shape resonance centered at 2.6 eV followed by a hump at 6.5 eV. The position of resonance is in close agreement with the experimental and theoretical value of 2.4 eV [22,39]. Thereafter, measurements and calculations of cross section decrease monotonically. Up to 7 eV, both our σ_{el} and σ_t results are similar to each other because the absorption potential becomes effective after the threshold energy. Our σ_t cross section results are in excellent agreement with the experimental measurements of Szmytkowski *et al.* [22] in the entire energy region. In Fig. 7(b) σ_{el} and σ_t cross sections are presented in the energy range from 20 to 100 eV. It has been noticed that our σ_t results continue to be in agreement with the experimental measurements of Szmytkowski *et al.* [22]. However, our calculated σ_t results are slightly lower than the measurements of Szmytkowski *et al.* [22].

Finally, elastic σ_m cross sections for the $e-PH_3$ systems are exhibited in Figs. 8(a) and 8(b). No experimental information is available for this parameter in this energy range. Present σ_m results are compared with the theoretical calculation of Yuan and Zhang [37], available at energies from 0.5 to 50 eV; and with that of Winstead *et al.* [32] in the energy range 1–40 eV. In Fig. 8(a), σ_m cross sections are illustrated in the energy range 0.1–20 eV. In this energy region, the σ_m curve exhibits similar behavior as exhibited in the calculation of Winstead *et al.* [32]. The results of Yuan and Zhang [37] also have similar shape but they differ in magnitude up to 9 eV. Beyond 10 eV, the difference is insignificant. For the sake of completeness, we have presented σ_m cross sections in the energy range 20–100 eV along with calculations of Winstead *et al.* [32] and Yuan and Zhang [37]. Our results are lower by 10% in comparison to Winstead *et al.* [32], which are available only up to 40 eV.

IV. CONCLUSIONS

We have presented our calculated elastic DCS, integral, and momentum-transfer cross sections along with total (elastic plus inelastic) cross sections for electrons scattering from NH_3 and PH_3 molecules at energies 0.1–100 eV. In these calculations, modified semiclassical exchange potential is used to account for the effect of exchange of the scattering electron and target electron along with a parameter-free correlation polarization potential which accounts for the polarization of a target charge cloud. The imaginary part is the absorption potential which is used to estimate the loss of flux into the inelastic channels. The exchange, a parameter-free correlation polarization, and static potentials are derived from the *ab initio* molecular charge density. A parameter-free spherical complex optical potential is treated exactly in the partial-wave scheme to obtain the various scattering parameters. Our main conclusions are as follows:

(i) The use of modified semiclassical exchange potential considerably improves the cross sections; thus results obtained compare well with available experimental measurements.

(ii) All the salient features (such as shape resonance and Ramsauer-Townsend minima) in the cross sections are reproduced well by the present theoretical calculation as observed in various measurements.

(iii) The inclusion of absorption potential as the imaginary part of the total optical potential makes it possible to compare our total (elastic plus inelastic) cross sections for both molecules with the available experimental data above the threshold energy. Further, it is noticed that due to absorption potential, elastic cross sections decrease significantly at impact energies beyond 15 eV.

(iv) The absorption potential is not effective at lower angles for DCS where most of the contribution comes through the polarization potential.

Finally, there is a need of experimental progress for $e-PH_3$ collisions for the assessment of present results, especially on the DCS and momentum-transfer cross sections. Our calculated DCS may provide a benchmark for future experimental measurements.

ACKNOWLEDGMENT

We gratefully acknowledge the financial support for this research work from Department of Science and Technology (DST), New Delhi, India, under Project No. SR/S2/LOP-0015/2010(G).

[1] P. G. J. Irwin, *Giant Planets of our Solar System: Atmospheres, Composition and Structure*, 2nd ed. (Springer Praxis Books, New York, 2009), and references therein.

[2] See, for example, *Swarm Studies and Inelastic Electron Molecule Collisions*, edited by L. C. Pitchford, B. V. McKoy, A. Chutjian, and S. Trajmar (Springer-Verlag, New York, 1987).

[3] Z. Xiaming, W. Huizhen, W. Shuangjiang, Z. Yingying, C. Chunfeng, S. Jianxiao, Y. Zijian, D. Xiaoyang, and D. Shurong, J. Semicond. **30**, 033001 (2009).

[4] M. Fuechsle, J. A. Miwa, S. Mahapatra, H. Ryu, S. Lee, O. Warschkow, L. C. L. Hollenberg, G. Klimeck, and M. Y. Simmons, Nat. Nanotechnol. **7**, 242 (2012).

[5] M. Y. Simmons, F. J. Ruess, K. E. J. Goh, T. Hallam, S. R. Schofield, L. Oberbeck, N. J. Curson, A. R. Hamilton, M. J. Butcher, R. G. Clark, and T. C. G. Reusch, Mol. Simulat. **31**, 505 (2005).

[6] L. N. Fletcher, K. H. Baines, T. W. Momary, A. P. Showman, P. G. J. Irwin, G. S. Orton, M. Roos-Serote, and C. Merlet, Icarus **214**, 510 (2011).

[7] D. Glindemann, M. Edwards, and P. Kuschk, Atmos. Environ. **37**, 2429 (2003).

[8] Th. Encrenaz, B. Bézard, J. Crovisier, A. Coustenis, E. Lellouch, S. Gulkis, and S. K. Atreya, Planet. Space Sci. **43**, 1485 (1995).

[9] X. Niu, A. Wei, Y. Li, L. Mi, Z. Yang, and X. Song, Chemosphere **93**, 1942 (2013).

[10] K. Shigemura, M. Kitajima, M. Kurokawa, K. Toyoshima, T. Odagiri, A. Suga, H. Kato, M. Hoshino, H. Tanaka, and K. Ito, Phys. Rev. A **89**, 022709 (2014).

[11] L. Chiari, A. Zecca, E. Trainotti, G. García, F. Blanco, M. H. F. Bettega, S. d'A. Sanchez, M. T. do N. Varella, M. A. P. Lima, and M. J. Brunger, Phys. Rev. A **88**, 022708 (2013).

[12] K. Anzai, H. Kato, M. Hoshino, H. Tanaka, Y. Itikawa, L. Campbell, M. J. Brunger, S. J. Buckman, H. Cho, F. Blanco, G. Garcia, P. Limão-Vieira, and O. Ingólfsson, Eur. Phys. J. D **66**, 36 (2012).

[13] O. Sueoka, S. Mori, and Y. Katayama, J. Phys. B: At. Mol. Phys. **20**, 3237 (1987).

[14] D. T. Alle, R. J. Gulley, S. J. Buckman, and M. J. Brunger, J. Phys. B: At. Mol. Opt. Phys. **25**, 1533 (1992).

[15] Cz. Szmytkowski, K. Maciag, G. Karwasz, and D. Filipovic, J. Phys. B: At., Mol. Opt. Phys. **22**, 525 (1989).

[16] N. C. Jones, D. Field, S. L. Lunt, and J. P. Ziesel, Phys. Rev. A **78**, 042714 (2008).

[17] Y. Itikawa, At. Data Nucl. Data Tables **14**, 1 (1974).

[18] J. W. Otvos and D. P. Stevenson, J. Am. Chem. Soc. **78**, 546 (1956).

[19] T. D. Mark and F. Egger, J. Chem. Phys. **67**, 2629 (1977).

[20] W. M. Ariyasinghe, T. Wijerathna, and D. Powers, Phys. Rev. A **68**, 032708 (2003).

[21] P. G. Millican and I. C. Walker, J. Phys. D: Appl. Phys. **20**, 193 (1987).

[22] Cz. Szmytkowski, L. Klosowski, A. Domaracka, M. Piotrowicz, and E. Ptasińska-Denga, J. Phys. B: At., Mol. Opt. Phys. **37**, 1833 (2004).

[23] H. Munjal and K. L. Baluja, Phys. Rev. A **74**, 032712 (2006).

[24] A. Jain, J. Phys. B: At., Mol. Opt. Phys. **21**, 905 (1988).

[25] J. L. S. Lino, Rev. Mex. Fis. **51**, 100 (2005).

[26] H. P. Pritchard, M. A. P. Lima, and V. McKoy, Phys. Rev. A **39**, 2392 (1989).

[27] F. A. Gianturco, J. Phys. B: At., Mol. Opt. Phys. **24**, 4627 (1991).

[28] T. N. Rescigno, B. H. Lengsfield, C. W. McCurdy, and S. D. Parker, Phys. Rev. A **45**, 7800 (1992).

[29] J. Yuan and Z. Zhang, Phys. Rev. A **45**, 4565 (1992).

[30] A. Jain and D. G. Thompson, J. Phys. B: At. Mol. Phys. **16**, 2593 (1983).
[31] A. K. Jain, A. N. Tripathi, and A. Jain, Phys. Rev. A **39**, 1537 (1989).
[32] C. Winstead, Q. Sun, V. McKoy, J. L. S. Lino, and M. A. P. Lima, Z. Phys. D: At., Mol. Clusters **24**, 141 (1992).
[33] M. H. F. Bettega and M. A. P. Lima, J. Phys. B: At., Mol. Opt. Phys. **37**, 3859 (2004).
[34] M. H. F. Bettega, M. A. P. Lima, and L. G. Ferreira, J. Chem. Phys. **105**, 1029 (1996).
[35] M. T. do N. Varella, M. H. F. Bettega, A. J. R. da Silva, and M. A. P. Lima, J. Chem. Phys. **110**, 2452 (1999).
[36] C. Limbachiya, M. Vinodkumar, and N. Mason, Phys. Rev. A **83**, 042708 (2011).
[37] J. Yuan and Z. Zhang, Z. Phys. D: At., Mol. Clusters **28**, 207 (1993).
[38] A. Jain and K. L. Baluja, Phys. Rev. A **45**, 202 (1992).
[39] H. Munjal and K. L. Baluja, J. Phys. B: At., Mol. Opt. Phys. **40**, 1713 (2007).
[40] F. A. Gianturco and D. G. Thompson, Chem. Phys. **14**, 111 (1976).
[41] A. Jain and D. G. Thompson, J. Phys. B: At. Mol. Phys. **20**, 2861 (1987).
[42] A. Jain, Phys. Rev. A **34**, 3707 (1986); J. Phys. B: At., Mol. Phys. **19**, L807 (1986).
[43] A. Jain, J. Chem. Phys. **86**, 1289 (1987).
[44] F. A. Gianturco and A. Jain, Phys. Rep. **143**, 347 (1986).
[45] F. A. Gianturco and S. Scialla, J. Phys. B: At. Mol. Phys. **20**, 3171 (1987).
[46] J. K. O'Connell and N. F. Lane, Phys. Rev. A **27**, 1893 (1983).
[47] N. T. Padial and D. W. Norcross, Phys. Rev. A **29**, 1590 (1984).
[48] F. A. Gianturco, A. Jain, and L. C. Pantano, J. Phys. B: At. Mol. Phys. **20**, 571 (1987).
[49] F. Blanco and G. Garcia, Phys. Lett. A **255**, 147 (1999).
[50] M.-T. Lee, I. Iga, L. E. Machado, and L. M. Brescansin, Phys. Rev. A **62**, 062710 (2000).
[51] G. Staszewska, D. W. Schwenke, D. Thirumalai, and D. G. Truhlar, J. Phys. B: At. Mol. Phys. **16**, L281 (1983).
[52] F. Calagero, *Variable Phase Approach to Potential Scattering* (Academic, New York, 1974).